49th AIAA Aerospace Sciences Meeting including the New Horizons Forum and Aerospace Exposition
4 - 7 January 2011, Orlando, Florida

Kinetic Effects of Non-Equilibrium Plasma on Partially Premixed Flame Extinction

Wenting Sun[1] Mruthunjaya Uddi[2] Sang Hee Won[3] Yiguang Ju[4]
Princeton University, Princeton, NJ 08544

and

Timothy Ombrello[5] Campbell Carter[6]
U.S. Air Force Research Laboratory, Propulsion Directorate, Wright-Patterson AFB, OH, 45433

A new plasma assisted combustion system was developed by integrating a counterflow burner with nano-second pulsed non-equilibrium discharge. The kinetic effects of plasma assisted fuel oxidization on the extinction of partially premixed methane flames was studied at 60 Torr by blending 2% CH_4 into the oxidizer stream. The non-equilibrium discharge accelerated dramatically the fuel oxidation. The O production and the products of plasma assisted fuel oxidation were measured, respectively, by using two-photon absorption laser-induced fluorescence (TALIF) method, Fourier Transform Infrared (FTIR) spectrometer , and Gas Chromatography (GC). The product concentrations were used to validate an existing plasma assisted combustion kinetic model. The comparisons showed the kinetic model prediction was poor due to missing reaction pathways, such as those involving carbon formation, H_2 excitation and dissociation, and interactions of excited species with hydrocarbon species. The path flux analysis determined that O was the critical species for kinetic modeling because it was generated by the discharge and dictated the oxidization process. The extinction strain rate measurements showed the non-equilibrium plasma discharge extended the extinction limit significantly. Strong emission from Ar* was observed at high plasma repetition rates and numerical modeling showed that Ar* contributed significantly to the enhancement of extinction limit.

Nomenclature

a	=	extinction strain rate
a_{21}	=	fluorescence quantum yields
f	=	pulser repetition frequency
$FWHM$	=	full-width half-maximum
$F_O(T)$	=	atomic oxygen Boltzmann factor
L	=	separation distance between two nozzles of counterflow burner
P	=	pressure
S_i	=	observed signal
T	=	temperature
U_O	=	velocity of oxidizer side
U_f	=	velocity of fuel side
V_P	=	peak voltage of the pulser

[1] Graduate student, Dept. Mechanical and Aerospace Engineering, EQUAD on Olden Street, Student Member.
[2] Post-doctoral Research Associate, Dept. of Mechanical and Aerospace Engineering, EQUAD on Olden Street, Member.
[3] Associate Research Scholar, Dept. of Mechanical and Aerospace Engineering, EQUAD on Olden Street, Member.
[4] Associate Professor, Dept. of Mechanical and Aerospace Engineering, EQUAD on Olden Street, Associate Fellow.
[5] Research Aerospace Engineer, Aerospace Propulsion Division, 1950 Fifth Street, Member AIAA.
[6] Principal Aerospace Engineer, Aerospace Propulsion Division, 1950 Fifth Street, Associate Fellow AIAA.

X_f = fuel mole fraction
X_O = oxygen mole fraction
υ_i = photon energy
ρ_O = oxidizer density
ρ_f = fuel density
$\sigma^{(2)}$ = two photon absorption cross section

I. Introduction

Over the last few years, plasma assisted combustion has drawn more and more attention for its potential to enhance combustion performance in gas turbines and scramjet engines. Extensive efforts have been made to understand the kinetic processes in plasma-flame interaction.[1-17] However, since plasma produces heat, radicals, excited species, ions/electrons, and other intermediate species simultaneously, one of the major challenges is to decouple the complex plasma-flame interaction so that the contribution of individual species produced by plasma to enhance combustion can be understood quantitatively at the elementary reaction level. As such, it is of great importance to develop well-defined plasma-combustion systems that can provide quantitative, fundamental experimental data to understand the effects of plasma generated species and validate plasma-assisted combustion kinetic mechanisms.

Recently many experimental studies have been carried to understand the role of plasma generated species on ignition, flame stabilization, and extinction. For ignition studies, the reduction of ignition temperature was confirmed and analyzed in a counterflow burner with the activation by a magnetic gliding arc.[1] The catalytic effect of NO_x on ignition enhancement was quantitatively examined. The reduction of ignition delay time by a non-equilibrium plasma discharge was also measured in Refs. [11, 18]. The results showed that the ignition delay times could be decreased by about an order of magnitude with the action of plasma. An increase of atomic oxygen concentration was observed and was used as an explanation for the decrease of ignition delay times. For plasma assisted flame speed enhancement, quantitative understanding of the enhancement mechanism of flame speed by plasma produced species has been investigated by several research groups.[12, 15, 16, 19] Ombrello and co-workers isolated singlet oxygen ($O_2(a^1\Delta_g)$) and ozone (O_3) effects and demonstrated that both (at concentrations of several thousand ppm) enhanced flame speeds by a few percent.[15, 16] The experimental data further showed that the current kinetic model for $O_2(a^1\Delta_g)$ significantly over-predicted the enhancement for hydrocarbon flames. Enhancement of flame stability by non-equilibrium plasma discharge and an electric field in a partially premixed mixture also has been observed for lifted flames.[13, 14, 20] Different explanations have been given based on the production of H_2 and CO as well as the formation of H and O and the ionic wind. Unfortunately, few experiments have been conducted to understand the mechanism of the extension of extinction limit by plasma discharge. Recently, our plasma assisted diffusion flame extinction experiment[17] showed a dramatic enhancement of extinction limit due to the production of atomic oxygen by a nano-second pulsed plasma discharge. However, in this experiment, the plasma discharge was limited to the oxidizer stream. The experiments did not provide any kinetic data for plasma assisted fuel oxidation for understanding and validating the plasma flame kinetic mechanism. As such, it is not clear how plasma assisted fuel oxidization affects the extinction of partially premixed fuel and oxidizer. Moreover, it remains unknown whether the current plasma mechanism[8] can reproduce the experimental data.

The goal of the present study was to study the effect of plasma assisted fuel oxidization on extinction of partially premixed methane flames at sub-atmospheric pressure by using a counterflow geometry. At the same time, quantification of the plasma assisted oxidization products provided data to improve the predictive capability of our plasma assisted combustion kinetic mechanism. Thus, the concentration of atomic oxygen was measured using a Xenon calibrated, two photon absorption laser induced fluorescence (TALIF) method. Furthermore, the concentrations of stable products from the plasma assisted fuel oxidation were measured by Fourier Transform Infrared spectroscopy (FTIR) and Gas Chromatography (GC). These experimental data were used to validate our current plasma flame chemistry model through the comparison between experiment and prediction.[8, 21]

II. Experimental Methods and Kinetic Modeling

A. Partially Premixed Counterflow Flame System with Nano-Second Plasma Discharge

A schematic of the experimental system is shown in **Fig. 1**. The setup consisted of a counterflow burner that was located in a vacuum chamber with a respective diameter and height of 406 and 629 mm. The inner diameters of the reactant and coflow nozzles were 20 and 28 mm, respectively, while the separation distance of the opposed nozzles was 20 mm. The inert curtain provided the isolation of the flame from the environment and burner cooling as well.

A honeycomb piece was placed inside the reactant nozzles to ensure that the flow field was uniform. The counterflow nozzles were made of quartz, and two parallel bare copper electrodes were located inside the tubes of the partially premixed upper nozzle. The ends of the electrodes were 10 mm away from the exit to avoid electric interaction with the thermocouple and allow the diffusion to smooth any non-uniformity. Because the pressure was only 60 Torr, diffusion was sufficiently fast and the effect of electrode on the flow field inside the tube was negligible. The electrodes were 15 mm × 22 mm size and were separated by 10 mm; furthermore, the electrode edges were smoothed to avoid the concentration of electric field and dielectric breakdown. To ensure that the flame was in the middle of the two burner exits, the momenta of the two reactant streams were matched. During the experiments, the partially premixed oxidizer stream composition was fixed as O_2/Ar/He/CH_4 (0.26:0.32:0.4:0.02). The fuel stream is CH_4 diluted by argon (fuel mole fraction varied from 0.2 to 0.4). A nano-second pulse generator (FPG 30-50MC4 from FID) was used to generate the non-equilibrium plasma, which was capable of producing 32 kV pulses with individual pulse duration of 12 ns, full width at half maximum (FWHM). The frequency of the pulser was adjustable from 1 to 50 kHz. A typical voltage waveform is shown in **Fig. 2** and was measured by a LeCroy high voltage probe (PPE20KV). The current through the electrodes was measured with a Pearson Coil (Model 6585). The pulse energy supplied to the discharge was estimated from the time integral of the voltage and current and was approximately 1.27 mJ, corresponding to average powers of 5.1, 12.7, 25.4, 38.1 and 50.8 W at the respective frequencies of 4, 10, 20, 30 and 40 kHz. The amplitude of the voltage was fixed at 5.3 kV, as shown in **Fig. 2**. Typical pictures of the discharges are shown in **Fig. 3 (a)-(d)** at different repetition frequencies, respectively.

The extinction strain rates were measured by fixing the fuel mole fraction and increasing the flow velocity gradually until extinction occurred. At the same time, temperatures at the burner exits were measured using thermocouples. One thin wire thermocouple was fixed at the exit of the lower fuel burner, and the other thermocouple was movable and used to monitor the temperature at the exit of the upper burner. The thermocouple was coated with MgO and covered with grounded Nickel-Chrome sheath to remove the electromagnetic interference from the discharge.

B. Fourier Transform Infrared Spectroscopy (FTIR) and Gas Chromatography (GC) for Species Measurements

The major products (CH_4, CO, CO_2, CH_2O, and H_2O) from the plasma assisted fuel oxidation in the oxidizer stream were measured by a Fourier Transform Infrared (FTIR) spectrometer (Nicolet Magna-IR 550). A quartz probe with an inlet diameter 1 mm was placed axially at the oxidizer side nozzle exit and was attached to a heated line (to avoid H_2O condensation) of the FTIR spectrometer. The pressure and temperature in the FTIR system was held constant at 31 Torr and 120 ^oC. For H_2 measurement, a micro Gas Chromatography system (INFICON 3000) was used. The measurements had relative uncertainties less than 1% for CH_4, CO, CO_2 and 5% for H_2O and H_2. The uncertainty of the CH_2O measurement is 80 ppm.

C. Two-Photon Absorption Laser Induced Fluorescence (TALIF) System

Xenon calibrated, TALIF was used to measure the absolute atomic oxygen concentration at the oxidizer side burner exit.[8, 17] More detailed descriptions about TALIF method can be found in Ref. [22, 23], and only a summary of this method is presented here. Ground state atomic oxygen can be excited by absorbing two photons at a wavelength of 225.7 nm. The transition between the excited 3p ^3P state and the 3s ^3S state will release a single photon at 844.6 nm. Xenon can be excited from $5p^6\ ^1S_0$ to $6p'[3/2]_2$ with the two photons at 224.31 nm; de-excitation to $6s'\ [1/2]_1$ corresponds to fluorescence at 834.91 nm. The number density of atomic oxygen N_O was calculated using the following equation in terms of the known number density of Xenon, N_{Xe},[8]

$$N_O = \frac{S_O}{S_{Xe}} g_{ND} \frac{a_{21}(Xe)}{a_{21}(O)} \left(\frac{\sigma^{(2)}(Xe)}{\sigma^{(2)}(O)} \right) \left(\frac{\upsilon_O}{\upsilon_{Xe}} \right)^2 \times \frac{1}{F_O(T)} N_{Xe}$$

where S_o and S_{Xe} are the observed fluorescence signals for atomic oxygen and Xenon, respectively, a_{21} the fluorescence quantum yields, $\sigma^{(2)}$ the two photon absorption cross sections of Xe and O, $F_O(T)$ the atomic oxygen Boltzmann factor for the lower level of the two photon absorption, υ_i the photon energies, and g_{ND} the neutral density filter factor. These values can be found in Refs. [8, 23].

The schematic of the TALIF system is shown in **Fig. 4**. An Nd:YAG laser was used to generate 532 nm to pump a tunable dye laser operating at ~573 nm. This 573 nm beam was frequency doubled and mixed with the 1064 nm beam of the Nd:YAG laser to get a ~226 nm beam of ~ 10 μJ/pulse required for the TALIF diagnostics. The TALIF signal was observed using an 850 nm bandpass filter of 40 nm FWHM and a Hamamatsu photomultiplier (R636-10). Atomic oxygen was measured at a location 1 cm downstream from the electrode end (at the exit of the burner). Note that the UV beam was focused 30 mm ahead of the probe region to avoid saturation, using a 300 mm UV lens.

The dye laser was scanned to generate the atomic oxygen fluorescence spectrum. A separate vacuum cell was used to obtain the Xenon atom two-photon fluorescence spectrum. Corrections for the transmission of the vacuum cell and bandpass filter were made to find the atomic oxygen density by the method described in Refs. [8, 23].

D. Kinetic modeling

The kinetic model used in this work was an integration of the air plasma model[8] together with USC Mech II[24]. In addition, additional elementary reactions involving the dilution gases (He/Ar) were added (Table 1). The plasma combustion model incorporates a set of species conservation equations for number densities of neutral, charged, and excited species produced in the plasma, O, O_2, O_3, e, O_2^+, O^+, O^-, O_2^-. $O_2(a^1\Delta_g)$, $O_2(b^1\Sigma)$, $O(^1D)$, Ar(+), Ar(1), Ar(2), Ar(3) (Ar* for simplicity, with excitation energy 11.3, 11.6, and 12.9 eV), He(+), He(23S), He(21S), He(23P), He(21P), He(3SPD), He(4SPD), He(5SPD) (He* for simplicity, with excitation energy 19.8, 20.6, 21, 21.2, 22.9, 23.7, 24, and 24.5 eV), as well as the energy conservation equation for prediction of the temperature of the mixture. This set of equations are coupled with the steady, two-term expansion Boltzmann equation for the electron energy distribution function (EEDF) of the plasma electrons using experimentally measured cross sections of electron impact electronic excitation, dissociation, ionization, and dissociative attachment processes. The Boltzmann equation calculates the rate coefficients of the electron impact elementary reactions by averaging the cross sections over the EEDF. The kinetic model also incorporates chemical reactions of excited electronic species, electron-ion recombination and ion-ion neutralization processes, ion-molecule reactions, and electron attachment and detachment processes. Note that the present model does not solve the Poisson equation for the electric field and therefore does not take into account charge separation and sheath formation near the electrode. So in the present work, the reduced electrical field in the plasma was considered to be an adjustable parameter, varied until the CH_4 concentration matched with the experimental results at the burner exit. More details about this model could be found at Refs. [21, 25].

Table I. List of Ar/He related reactions involved in Ar/He/O_2/CH_4 mixture discharge

Reaction	Rate (cm^3s^{-1})	Reference
Ar + e = Ar* + e	σ^a	[26]
Ar + e = Ar(+) + 2e	σ	[26]
Ar* + O_2 = Ar + 2O	2×10^{-10}	[26]
Ar(+) + O_2 = Ar + O_2(+)	1×10^{-10}	[26]
Ar* + CH_4 = Ar + CH_2 + 2H	3.3×10^{-10}	[26]
Ar* + CH_4 = Ar + CH + H_2 + H	5.8×10^{-10}	[26]
Ar* + CH_4 = Ar + CH_3 + H	5.8×10^{-10}	[26]
Ar* + CH_4 = Ar + CH_2 + H_2	5.8×10^{-10}	[26]
Ar(+) + CH_4 = Ar + CH_3(+) + H	6.5×10^{-10}	[26]
Ar(+) + CH_4 = Ar + CH_2(+) + H_2	1.4×10^{-10}	[26]
He + e = He* + e	σ	[27]
He + e = He(+) + 2e	σ	[27]
He + $O(^1D)$ = He + O	1×10^{-10}	[28]
He* + O_2 = He + O_2(+) + e	$1.5\times10^{-11}T^{0.5}$	[27]
He* + O = He + O(+) + e	$1.5\times10^{-11}T^{0.5}$	[27]
He(+) + O_2 = He + O(+) + O	$0.6\times10^{-11}T^{0.5}$	[27]
He(+) + O_3 = He + O_2 + O	$0.6\times10^{-11}T^{0.5}$	[27]
He(+) + $O_2(a^1\Delta_g)$ = He + O(+) + O	$0.6\times10^{-11}T^{0.5}$	[27]
He(+) + $O(^1D)$ = He + O(+)	$2.9\times10^{-12}T^{0.5}$	[27]
He + 2O = He* + O_2	1×10^{-33}	[27]
He* + CH_4 = He + CH + H_2 + H	5.6×10^{-13}	[29]

[a]The rate is calculated by the Boltzmann solver using an experimentally measured cross-section, σ

III. Results and Discussion

A. Effects of plasma repetition rate on species concentrations from plasma assisted fuel oxidization

FTIR was used to quantify the most products of plasma assisted fuel oxidization in the oxidizer stream. Typical FTIR absorption spectra are shown in **Fig. 5 (a)-(f)**. **Fig. 5 (a)** shows the results without the discharge. The CH_4

absorbance spectrum is seen clearly without any effects from ambient CO_2 and H_2O. With the presence of the plasma discharge, absorbance spectra of CO, CO_2, H_2O and CH_2O appeared due to the plasma assisted fuel oxidization. Moreover, as shown in **Fig. 5 (b)-(f)**, with the increase of discharge pulse repetition frequency, the concentrations of CO, CO_2 and H_2O increased significantly, and at the same time, the concentration of CH_4 decreased. The dependence of the measured concentrations of CO, CO_2, H_2, H_2O and CH_2O on the plasma pulse repetition rate is shown in **Figs. 6– 8.** In order to validate the plasma flame model, the predicted species concentrations are also plotted in **Figs. 7 and 8.** In all the FTIR measurements, it was confirmed that the carbon closure with the measured species was 95%, demonstrating that the measurements captured the major carbon containing species in the plasma assisted fuel oxidation. It was also observed that the minor carbon loss was caused by carbon black formation in the plasma discharge. As shown in **Figs. 6** and **7**, with the increase of pulse repetition frequency, the CH_4 concentration decreased significantly, and nearly 90% of CH_4 was oxidized at pulse repetition frequency f= 40 kHz. At the same time, the concentrations of CO, CO_2 and H_2O increased monotonically with f. Note that the concentration of H_2 increased at low repetition frequency but then decreased at high frequency. The peak concentration of H_2 occurred at pulse repetition frequency f= 20 kHz. A similar trend was found for CH_2O with peak concentration at f= 10 kHz, as shown in **Fig. 8**. It is shown in both **Figs. 7** and **8** that the model captured the right trend of the relationship between the species concentrations and pulse repetition frequency, but the kinetic model over-predicted CO, CH_2O and H_2, and under-predicted CO_2, indicating that the model underestimated the overall reactivity of the oxidizer stream. This may indicate that the kinetic mechanism is missing some reaction paths that accelerate the oxidization process of the fuel. Notably, during the experiments, carbon black is formed (on the electrode), but the formation of C_2 is not predicted by the kinetic model. C_2 may arise from electron and Ar* collisions that further dissociate CH_2, CH or CH_3 based on reaction (1) to (6), such as e + CH = C + H +e. C_2 can be oxidized to CO through reactions with OH or O_2 to generate radicals H or O. These reactions can accelerate the oxidization process of the fuel and improve the model prediction.

In order to understand the plasma assisted fuel oxidization mechanism better, a path flux analysis was performed for a pulse repetition frequency f= 40 kHz, as shown in **Fig. 9**. CH_4 was mainly dissociated to CH_3 by H abstraction with OH, O and H. It also decomposed to CH_3, CH_2 and CH via collisions with an electron, Ar(+) and Ar* (reactions (1)-(6)). The formed CH_3, CH_2 and CH were further oxidized to CH_2O, HCO, CO and finally CO_2 as shown in **Fig. 9 (a)**. Among those reaction paths, a total of 12% of CH_4 was decomposed by collisions with an electron, Ar(+) and Ar*. H_2 is an important product of plasma assisted fuel oxidation because it affects greatly the ignition and extinction process via fast chemistry. The reaction path of H_2 is shown in **Fig. 9 (b)**. The dominant formation path of H_2 was through H abstraction reactions with species such as CH_4, CH_2O, HO_2, HCO, CH_2 and CH_3. Another formation path of H_2 was through CH_4 decomposition by Ar*, but only about 1% of H_2 was formed through this path. Therefore, H concentration is important to determine the concentration of H_2. The reaction paths of H and O are also shown in **Fig. 10 (a)** and **(b)**. As shown in **Fig. 10 (a)**, only 11.7% H was formed during the decomposition of CH_4 through reactions (1) to (5). The major contribution to H formation was from reaction CH_3 + O = CH_2O + H.

$$CH_4 + e = CH_3 + H + e \quad (1)$$
$$CH_4 + Ar(+) = CH_3(+) + H + Ar \quad (2)$$
$$CH_4 + Ar^* = CH_2 + H + H + Ar \quad (3)$$
$$CH_4 + Ar^* = CH_3 + H + Ar \quad (4)$$
$$CH_4 + Ar^* = CH + H_2 + H + Ar \quad (5)$$
$$CH_4 + Ar^* = CH_2 + H_2 + Ar \quad (6)$$

The reaction path of O is shown in **Fig. 10 (b)**. Approximately 66% of O was formed through collisions between O_2 and electrons, Ar*, and He(+). Among these reaction paths, 33% of O formation was from direct electron impact to dissociate O_2, while 20% of O formation was from O_2 collisions with Ar*. Once O was generated by the discharge, it was consumed rapidly by CH_4 and its intermediate oxidization and dissociation products (CH_3, CH_2, CH_2O, HCO, HO_2 and H_2). It is seen from **Fig. 10 (b)** that the major consumption path of O generated OH and H, which are very important to the fuel oxidization. Only 0.6% of O recombined to O_2. This indicated that when discharge was applied to the premixed fuel and oxidizer, O can be consumed more efficiently by the fuel and its intermediate oxidization and dissociation products than through recombination. Based on the above analysis, it is clear that O production of plasma discharge in a partially premixed fuel and oxidizer is critical for hydrogen formation and fuel oxidation in general. Therefore, in order to predict other species, O formation through the collision-induced O_2 dissociation by electrons and excited species needs to be accurately predicted.

In order to determine the concentration of atomic oxygen and compare with the kinetic model prediction, the Xenon calibrated, Two Photon Absorption Laser Induced Fluorescence (TALIF) method was used. The relationship between O concentration and pulse repetition frequency (for a flow velocity of 200 cm/s) is plotted in **Fig. 8**. As shown, with the increase of pulse repetition frequency, the O concentration increased but was relatively low, less than 300 ppm, even at *f*=40 kHz. As shown in **Fig. 10 (b)**, this is because of the consumption by the fuel and its intermediate oxidization and dissociation products in the partially premixed oxidizer stream. To demonstrate this, the O concentration without fuel was also measured by replacing the 2% CH_4 with Ar. The concentration of O increased sharply from 530 ppm to 2700 ppm when the pulse repetition frequency increased from 4 kHz to 40 kHz. The simulation results of O and CH_2O concentrations are also shown in **Fig. 8** together with the experimental measurements of CH_2O concentration. The calculated concentrations of O and CH_2O intersected with the experimental results and the deviations are maximized at *f*=40 kHz. The overall prediction of the kinetic model is poor, especially for O and CH_2O. A similar result was also reported in Ref. [7].

As analyzed, the model under-predicted the concentration of CO_2, and over-predicted CO, H_2O and H_2 which indicates overall lower reactivity of the mixture. For O and CH_2O prediction, the kinetic model under-predicted their concentrations at low pulse repetition frequency and over-predicted the concentrations at high pulse repetition frequency. The over-predicted O concentration may be caused by both production and consumption paths. At the one hand, 9.7% of O formation from $O_2(a^1\Delta_g)$ and $O_2(b^1\Sigma)$ may be over-estimated because of the lack of $O_2(a^1\Delta_g)$ and $O_2(b^1\Sigma)$ quenching reactions by hydrocarbon fuels (which are temperature dependent[30]). On the other hand, O should be consumed faster to accelerate the oxidization process. It is well known that O can be excited due to electron impact and O_2 dissociation reactions. Excited O is much more reactive especially at low temperature conditions. For example, the rate constant for $O(^1D) + H_2 = H + OH$ (1.1×10^{-10} cm^3/s)[31] is much larger than for $O + H_2 = H + OH$ (1.0×10^{-17} cm^3/s). Unfortunately, the reaction rates of excited O such as $O(^1D)$ with most hydrocarbon species are not well characterized and are absent in the current kinetic model. The formation of CH_2O was primarily from the reaction $CH_3 + O = CH_2O + H$. If O was over-predicted (or under-predicted), the concentration of CH_2O likewise would be over-predicted (or under-predicted). The over-prediction of CO and the under-prediction of CO_2 are likely due to missing reaction paths. As noted above, one missing reaction path was for carbon black formation and subsequent oxidization. For the over-prediction of H_2 concentration, excitation and dissociation of H_2 by electrons and Ar* should be considered. H_2* and H* are more reactive and thus could mitigate the deviation between experiments and simulations.

The kinetic model also showed the formation of C_2H_6 (~200 ppm), but the C_2H_6 absorption spectrum was not observed in the FTIR experiments. Previous research in a lean CH_4/air discharge [32] also showed no C_2H_6 formation, and thus the reaction $CH_3 + CH_3 = C_2H_6$ was over-estimated or the consumption path of C_2H_6 was under-estimated at low temperatures.

B. Extinction Strain Rates Measurement and Computation

The extinction strain rates of the CH_4/O_2 diffusion flames were measured without and with plasma (at *f*=4, 10, 20, 30, and 40 kHz). A definition of global strain rate[33]

$$a_O = \frac{2U_O}{L}\left(1+\frac{U_f\sqrt{\rho_f}}{U_O\sqrt{\rho_O}}\right) \qquad (1)$$

was adopted and compared with numerical simulations. Here U is the speed of the flow, ρ the density of the flow, and L the gap distance between the two nozzles. The subscript o and f refer to the oxidizer and fuel side, respectively.

In this experiment, the composition of partially premixed oxidizer stream was fixed at $CH_4/O_2/Ar/He$ ratio of 0.02/0.26/0.32/0.4. The fuel stream was CH_4/Ar mixture and the CH_4 concentrations varied from 0.2 to 0.4. During the measurements, the fuel mole fraction was fixed, and the flow velocity increased gradually. With the increase of flow velocity, the strain rate increased and the flame had less residence time to complete the fuel oxidation and extinguished when the strain rate was above a critical value. This critical strain rate at flame extinction was recorded as the global extinction strain rate. **Figure 11** shows the relationship of extinction strain rates and fuel mole fractions without plasma and with plasma at pulse repetition frequency of *f*=4 and 10 kHz (with oxidizer temperature T_o = 423±4 K and 613±5 K, respectively). The experimental results were further compared with numerical simulations. The simulation was computed by using OPPDIFF of the CHEMKIN package[34] with a modified arc-length continuation method[35] for plug flow. The mechanism used in the calculation was USC-Mech II[24] with addition of plasma related reactions discussed in section II. All simulations were performed by setting the boundary conditions using the measured temperatures, flow velocity, and species concentrations by FTIR, GC and TALIF. It is seen that with the increase of the pulse repetition frequency, there was a significant increase of extinction limit enhancement

and the experiments agree well with the simulations. The present results indicate that the plasma generated fuel oxidation plays an important role for the extension of flame extinction limit.

Previous research[13, 19, 36] showed that fuel reforming can enhance the flame stability. Therefore, it is very important to examine how the fuel reforming affects the extinction. Because plasma can cause both fuel oxidization and reformation, simulations of the individual effects of plasma assisted fuel oxidization and fuel reforming were done and shown in **Fig. 12**. In these simulations, part of the fuel (CH_4) in the oxidizer stream was assumed to be ideally oxidized to H_2O and CO_2 for Case 1, and ideally reformed to H_2 and CO in Case 2 under constant enthalpy constraint and at different extent (0% to 100%). We can see that extinction was enhanced for both cases, but the enhancement for the plasma assisted fuel oxidization case is much larger. This is because when the flame was approaching extinction, the residence time was too short to complete the reactions. That is, the fuel and its reformation products in the oxidizer stream cannot react completely to release the chemical enthalpy in Case 2, but the chemical enthalpy was already released in Case 1 before reaching the reaction zone.

The extinction strain rates measurements were also conducted at f = 20, 30 and 40 kHz (with oxidizer temperature T_o = 678±5 K, 775±5 K and 889±8 K, respectively and with measured boundary conditions as described above) by fixing the fuel mole fraction and are shown in **Fig. 13**. At f=10 kHz, the experimental measurement agree with the simulation, but with the increase in f, the experiments and simulations begin to deviate, which may indicate that there are additional reaction paths to enhance the flame extinction. The extinction strain rates at constant enthalpy condition with the original 2% CH_4 in the partially premixed oxidizer stream are also shown in **Fig.13** as a reference. With the further oxidization of CH_4 (increased f) in the partially premixed oxidizer stream, the extinction strain rates increased significantly.

As indicated in **Fig. 3**, when f was larger than 10 kHz, a visible plasma jet appeared. Emission spectroscopy (Ocean Optics, USB2000+ spectrometer) was employed to identify the possible products of the discharge excitation. Apertures and collimating lens were used to collect the emission in the afterglow region beneath the nozzle exit. The strongest emission was from Ar* at 750 nm, together with emissions from He*, O*, OH*, HCO* and CH*. The emission intensity from Ar* at 750 nm is shown at **Fig. 14** versus pulse repetition frequency. With the increase of pulse repetition, the Ar* emission in the afterglow region increased, indicating the increased concentration of Ar*. It is possible that the "missing" reaction path(s) affecting flame extinction involve Ar*. A preliminary test on the effect Ar* addition on extinction was performed by simulations and is shown in **Fig. 14**. In order to mitigate the deviation of extinction strain rates between the experiments and simulations, different amounts of Ar* were tried at different values of f. With the increase in f, more Ar* was required and the trend was similar to the emission intensity curve. Up to 7000 ppm of Ar* was required for the simulation to match with the experiments with f=40 kHz. Optical emission spectra also identified other species like He*, O*, H*, OH*, HCO* and CH*. However, quantitative measurements of Ar* and other species are challenging, and thus measurement of these species will be a focus for future research.

IV. Summary and Conclusions

A new well-defined platform to study the kinetic effects of non-equilibrium plasma on partially premixed flame extinction at low pressure was developed by integrating a counterflow burner with a nano-second pulsed discharge. The compositions of the partially premixed oxidizer stream after the activation of plasma was quantified by FTIR, GC and TALIF and compared with numerical kinetic modeling. The kinetic model over-predicted the concentrations of CO, H_2O, H_2 and under-predicted the concentration of CO_2. The predicted concentrations of O and CH_2O from the kinetic model intersected with the experimental results and the deviations are maximized at f=40 kHz. Reaction(s) involving carbon formation was absent in the kinetic mechanism, though carbon build-up on the electrodes was observed. This reaction path may be induced by collisions via electrons and Ar* with CH_2, CH or CH_3 that can accelerate the oxidization process of the fuel. The excitation and dissociation of H_2 should also be considered to mitigate the over-prediction of kinetic modeling. The reaction path analysis recognized that O was the critical species for kinetic modeling, because O was generated by the discharge and then consumed to generate OH and H, which determined the oxidization process of the fuel and H_2 formation. The possible reason for the over-prediction of O by the current mechanism is the over-estimation of $H + O_2(a^1\Delta_g)/O_2(b^1\Sigma)$ process and the missing consumption paths related to excited O.

The extinction strain rates were measured at different pulse repetition frequency and compared with simulations by setting the boundary conditions using the measured temperatures and species concentrations by FTIR, GC and TALIF. At low pulse repetition frequency (f= ≤10 kHz), the experiments agree well with simulations. The effect of fuel reforming versus plasma assisted fuel oxidation was also examined through numerical simulation. The results showed both fuel reforming and fuel oxidization can extend the extinction limit, but fuel oxidization has a larger

effect on the extinction enhancement. This is because plasma can oxidize the fuel and extract the chemical energy regardless of the equivalence ratio and flow residence time. The effect of fuel reforming on the extinction is through the fast H_2 chemistry, but the H_2 reactions still need to compete with residence time to finish the heat release process. Finally, at high pulse repetition frequency, a visible plasma jet appeared between the two nozzles and the flame extinction measurements deviated with simulations. Strong emission from Ar* (at 750 nm) was observed at high plasma repetition rates, and numerical modeling showed that Ar* contributed significantly to the enhancement of extinction limit.

Acknowledgments

This work was supported by the MURI research grant from the Air Force Office of Scientific Research and the grant FA9550-07-1-0136 under the technical monitor of program manager Dr. Julian Tishkoff. Wenting Sun thanks Francis Haas, Saeid Jahangirian, Joshua Heyne and Joe Lefkowitz from the Department of Mechanical and Aerospace Engineering, Princeton University for the help of FTIR and GC measurements.

References

[1]Ombrello, T., Ju, Y., and Fridman, A., "Kinetic Ignition Enhancement of Diffusion Flames by Nonequilibrium Magnetic Gliding Arc Plasma," *AIAA Journal*, Vol. 46, No. 10, 2008, pp. 2424-2433.

[2]Ombrello, T., Qin, X., Ju, Y., Gutsol, A., Fridman, A., and Carter, C., "Combustion Enhancement via Stabilized Piecewise Non-equilibrium Gliding Arc Plasma Discharge," *AIAA Journal*, Vol. 44, No. 1, 2006, pp. 142-150.

[3]Bozhenkov, S. A., Starikovskaia, S. M., and Starikovskii, A.Y., "Nanosecond Gas Discharge Ignition of H2-and CH4-containing Mixtures," *Combustion and Flame*, Vol. 133, 2003, pp. 133-146.

[4]Starikovskii, A. Y., Anikin, N. B., Kosarev, I. N., Mintoussov, E. I., Starikovskaia, S. M., and Zhukov, V. P., "Plasma-assisted combustion," *Pure Appl. Chem.*, Vol. 78, No. 6, 2006, pp. 1256-1298.

[5]Starikovskaia, S.M., "Plasma assisted ignition and combustion," *J. Phys. D: Appl. Phys.*, Vol. 39, 2006, pp. R265-R299.

[6]Lou, G., Bao, A., Nishihara. M., Keshav. S., Utkin. Y. G., Rich. J. W., Lempert, W. R., and Adamovich, I.V., "Ignition of premixed hydrocarbon–air flows by repetitively pulsed, nanosecond pulse duration plasma," *Proceedings of the Combustion Institute*, Vol. 31, 2007, pp. 3327-3334.

[7]Mintusov, E., Serdyuchenko, A., Choi, I., Lempert, W. R., and Adamovich, I. V., "Mechanism of Plasma assisted Oxidization and Ignition of Ethylene-air Flows by a Repetitively Pulsed Nanosecond Discharge," *Proceedings of the Combustion Institute*, Vol. 32, 2009, pp. 3181-3188.

[8]Uddi, M., Jiang, N., Mintusov, E., Adamovich, I. V., Lempert, W. R., "Atomic oxygen measurements in air and air/fuel nanosecond pulse discharges by two photon laser induced fluorescence," *Proceedings of the Combustion Institute*, Vol. 32, 2009, pp. 929-936.

[9]Pancheshnyi, S. V., Lacoste, D. A., Bourdon, A., and Laux, C. O., "Ignition of Propane–Air Mixture by a Repetitively Pulsed Nanosecond Discharge," *IEEE Trans. Plasma Sci.*, Vol. 34, No. 6, 2006, pp. 2478-2487.

[10]Chintala, N., Meyer, R., Hicks, A., Bao, A., Rich, J. W., Lempert, W. R., and Admovich, I. V., "Nonthermal ignition of premixed hydrocarbon-air flows by nonequilibriuim radio frequency plasma," *Journal of Propulsion and Power*, Vol. 21, No. 2, 2005, pp. 583-590.

[11]Kosarev, I. N., Aleksandrov, N. L., Kindysheva, S. V., Starikovskaia, S. M., Starikovskii, A. Y., "Kinetic mechanism of plasma-assisted ignition of hydrocarbons," *J. Phys. D: Appl. Phys.*, Vol. 41, 2008, p032002 (1-6).

[12]Starik, A. M., Kozlov, V. E., Titova, N. S., "On the influence of singlet oxygen molecules on the speed of flame propagation in methance-air mixture," *Combustion and Flame*, Vol. 157, 2009, pp. 313-327.

[13]Kim, W., Mungal, M. G, and Cappelli, M. A., "The role of *in situ* reforming in plasma enhanced ultra lean premixed methane/air flames," *Combustion and Flame*, Vol. 157, 2009, pp. 374-383.

[14]Pilla, G., Galley, D., Lacoste, D. A., Lacas, F., Veynante, D., and Laux, C. O., "Stabilization of a turbulent premixed flame using a nanosecond repetitively pulsed plasma," *IEEE Transactions on Plasma Science*, Vol. 34, No. 6, 2006, pp. 2471-2477.

[15]Ombrello, T., Won, S. H., Ju, Y., and Williams, S., "Flame propagation enhancement by plasma excitation of oxygen. Part I: effects of O_3," *Combustion and Flame*, Vol. 157, 2010, pp. 1906-1915.

[16]Ombrello, T., Won, S. H., Ju, Y., and Williams, S., "Flame propagation enhancement by plasma excitation of oxygen. Part I: effects of $O_2(a^1\Delta_g)$," *Combustion and Flame*, Vol. 157, 2010, pp. 1906-1915.

[17]Sun, W., Uddi, M., Ombrello, T., Won, S. H., Carter, C., and Ju, Y., "Effects of non-equilibrium plasma discharge on counterflow diffusion flame extinction," *Proc. Combust. Inst.*, 2010 (in press).

[18]Aleksandrov, N. L., Kindysheva, S. V., Kosarev, I. N., Starikovskaia, S. M., and Starikovskii, A. Y., "Mechanism of ignition by non-equilibrium plasma," *Proc. Combust. Inst.*, Vol. 32, 2009, pp. 205-212.

[19]Rao, X., Hemawan, K., Wichman, I., Carter, C., Grotjohn, T., Asmussen, J., and Lee, T., "Combustion dynamics for energetically enhanced flames using direct microwave energy coupling," Proc. *Combust. Inst.*, 2010 (in press).

[20]Won, S. H., Cha, M. S., Park, C. S., and Chung, S. H., "Effect of electric fields on reattachment and propagation speed of tribrachial flames in laminar coflow jets," Proc. *Combust. Inst.*, Vol. 31, 2007, pp. 963-970.

[21]Adamovich, I. V., Rich, J. W., and Nelson, G. L., "Feasibility Study of Magnetohydrodynamics Acceleration of Unseeded and Seeded airflows," A*IAA Journal*, Vol. 46, No. 10, 2008, pp. 2424-2433.

[22]Uddi, M., "Non-equilibrium kinetic studies of repetitively pulsed nanosecond discharge plasma assisted combustion," Ph.D. Dissertation, Mechanical Engineering Dept., Ohio State Univ., Columbus, OH, 2008.
[23]Niemi, K., Schulz-von der Gathen, V., and Dobele, H. F., "Absolute atomic oxygen density measurements by two-photon absorption laser-induced fluorescence spectroscopy in an RF-excited atmospheric pressure plasma jet," *Plasma Sources Sci. Technol.*, Vol. 14, 2005, pp. 375-386.
[24]Wang, H., You, X., Joshi, A.V., Davis, S.G., Laskin, A., Egolfopoulos, F., and Law, C. K., available at <http://ignis.usc.edu/USC_Mech_II.htm>
[25]Bao, A., "Ignition of hydrocarbon fuels by a repetitively pulsed nanosecond pulse duration plasma," Ph.D. Dissertation, Mechanical Engineering Dept., Ohio State Univ., Columbus, OH, 2008.
[26]Kosarev, I. N., Aleksandrov, N. L., Kindysheva, S. V., Starikovskaia, S. M., and Starikovskii, A. Y, "Kinetics of ignition of saturated hydrocarbons by nonequilibrium plasma: CH_4-containing mixtures," *Combustion and Flame*, Vol. 154, 2008, pp. 569-586.
[27]Stafford, D. S., and Kushner, M. J., "$O_2(^1\Delta)$ production in He/O_2 mixtures in flowing low pressure plasmas," *J. Appl. Phys.*, Vol. 96, 2004, pp2451-2465.
[28]Hicks, A., Norberg, S., Shawcross, P., Lempert, W. R., Rich, J. W., and Adamovich, I. V., "Singlet oxygen generation in a high pressure non-self-sustained electric discharge," *J. Phys. D: Appl. Phys.*, Vol. 38, 2005, pp. 3812-3824.
[29]Tsuji, M., Kobarai, K., Obase, H., Kouno, H., and Nishimura, Y., "Dissociative excitation of CH_4 by collisions with helium active species," *J. Chem. Phys.*, Vol. 94, 1994, pp277-282.
[30]Ombrello, T., Won, S. H., Ju, Y., Williams, S., and Campbell, C., "Mechanisms of kinetic combustion enhancement by $O_2(a^1\Delta_g)$," *48th AIAA Aerospace Sciences Meeting and Exhibit (2010)*, AIAA-2010-1586.
[31]Popov, N.A., "The Effect of nonequilibrium excitation on the ignition of hydrogen-oxygen mixtures," *High Temperature*, Vol. 45, 2007, pp. 261-279.
[32]Chintala, N., Lou, G., and Adamovich, I. V., "Measurements of combustion efficiency in nonequilibrium RF plasma-ignited flows," *Combustion and Flame*, Vol. 144, 2006, pp. 744-756.
[33]Seshadri, K., Williams, F. A., "Laminar Flow Between Parallel Plates with Injection of a Reactant at High Reynolds Number," *Int. J. Heat Mass Transfer*, Vol. 21, 1978, pp. 251-253.
[34]Kee, R. J., Rupley, F. M., Miller, J. A., Coltrin, M. E., Grcar, J. F., Meeks, E., Moffat, H. K., Lutz, A. E., Dixon-Lewis, G., Smooke, M. D., Warnatz, J., Evans, G. H., Larson, R. S., Mitchell, R. E., Petzold, L. R., Reynolds, W. C., Caracotsios, M., Stewart, W. E., Glarborg, P., Wang, C., Adigun, O., Houf, W. G., Chou, C. P., Miller, S. F., Chemkin Collection, Release 3.7.1, Reaction Design, Inc. 2003: San Diego, CA.
[35]Ju, Y., Guo, H., and Maruta, K, "On the extinction limit and flammability limit of non-adiabatic stretched methane-air premixed flames," *J. Fluid Mech.*, Vol. 23, 1997, pp. 315-334.
[36]Rao. X., Hammack, S., Lee, T., Carter, C., and Matveev, I. B., "Combustion Dynamics of Plasma-Enhanced Premixed and Nonpremixed Flames," IEE*E Trans. Plasma Sci.*, Vol. 38, No. 12, 2010, pp. 3265-3271.

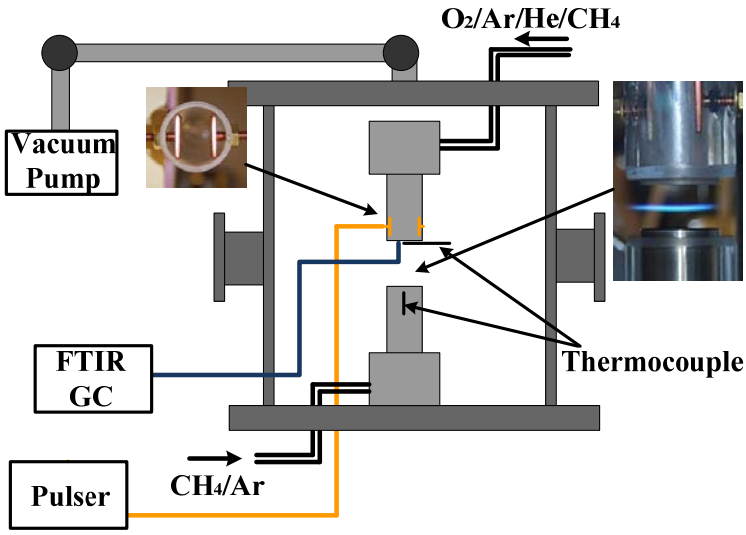

Figure 1. Schematic of experimental setup.

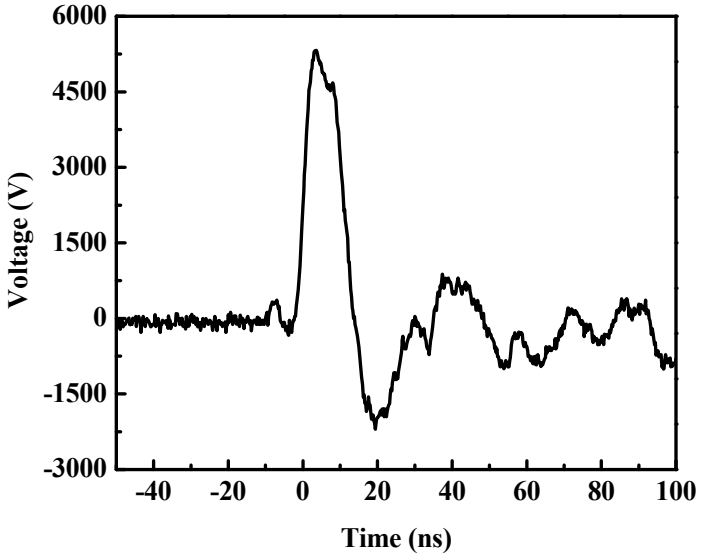

Figure 2. Typical voltage waveform produced by the nano-seconnd pulser.

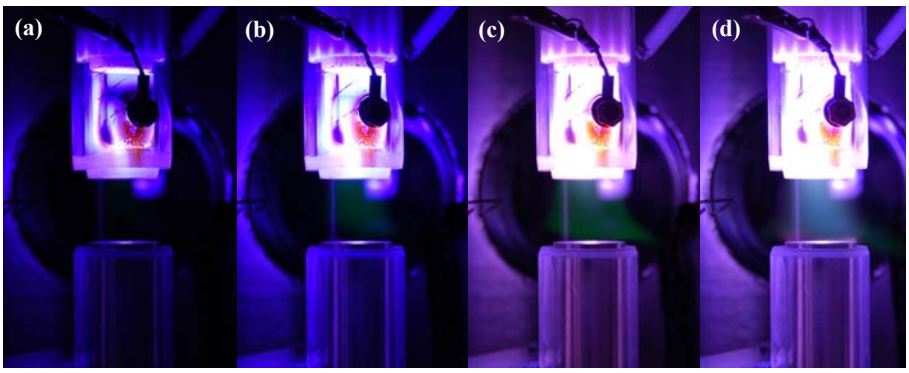

Figure 3. Pictures of discharges at Ar/He/O_2/CH_4(0.32/0.4/0.26/0.02), *d*=20 mm, *P*=60 Torr (a) *f*=10 kHz (b) *f*=20 kHz (c) *f*=30 kHz (d) *f*=40 kHz.

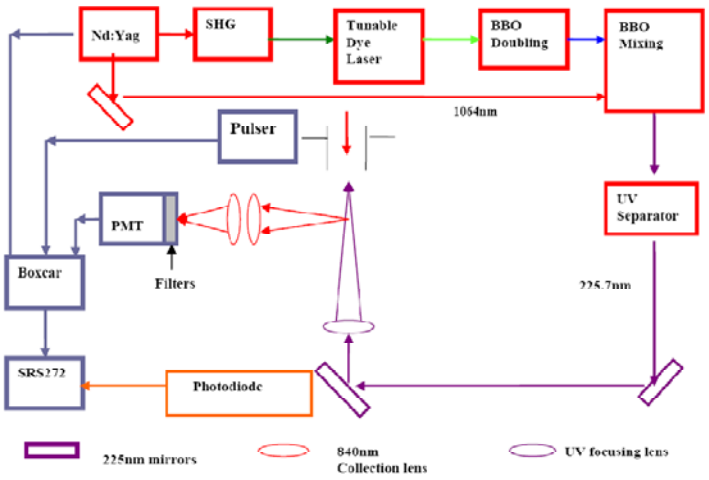

Figure 4. Schematic of the TALIF setup.

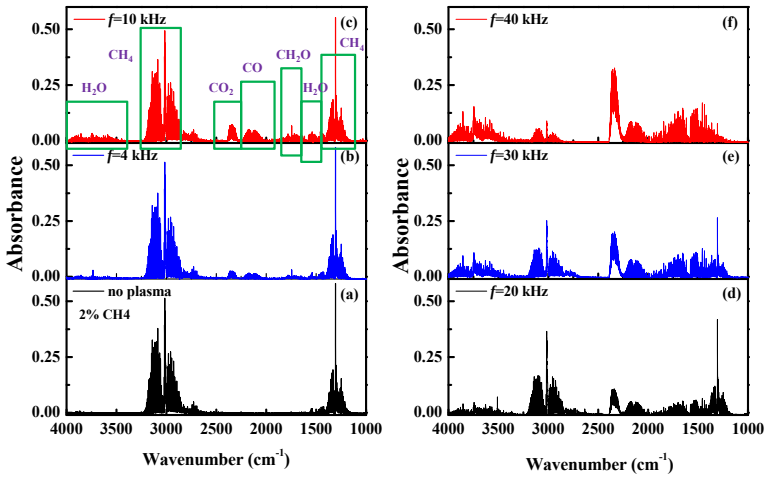

Figure 5. FTIR spectrum with different pulse repetition frequency at Ar/He/O_2/CH_4(0.32/0.4/0.26/0.02), *P*=60 Torr (a)no plasma (b) *f*=4 kHz (c) *f*=10 kHz (d) *f*=20 kHz (e) *f*=30 kHz (f) *f*=40 kHz.

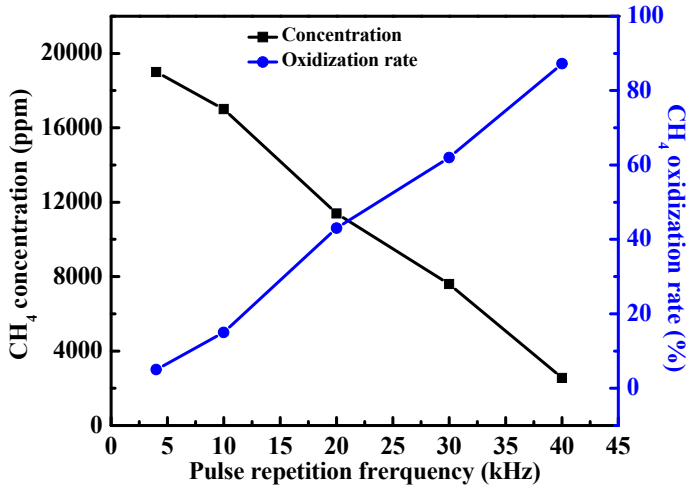

Figure 6. Relationship of CH_4 concentrations and oxidization ratios and pulse repetition frequency.

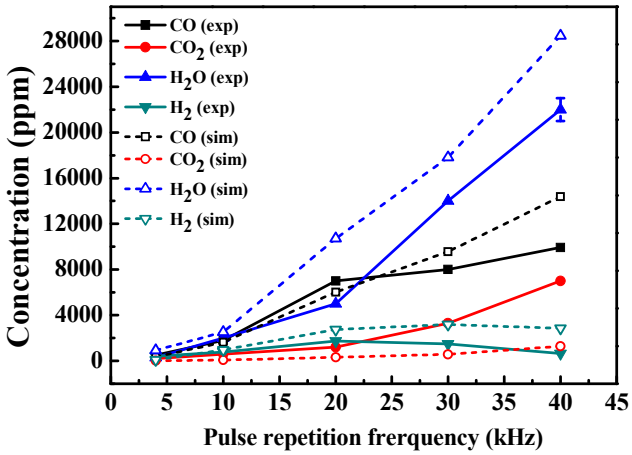

Figure 7. Relationship of species concentrations at the burner exit and pulse repetition frequency (experiments: solid symbol and line; simulations: empty symbol and dashed line).

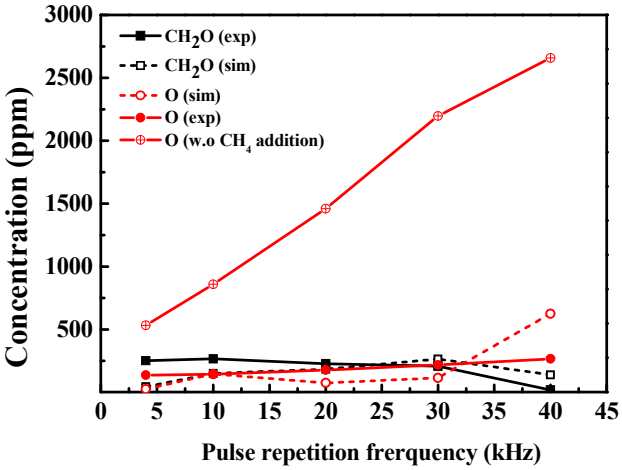

Figure 8. Relationship of species concentrations at the burner exit and pulse repetition frequency (experiments: solid symbol and line; simulations: empty symbol and dashed line).

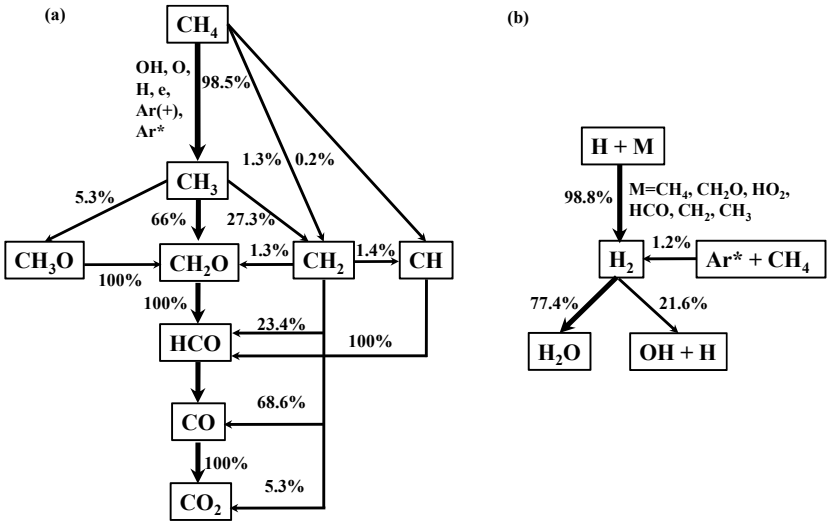

Figure 9. Reaction paths flux analysis for (a) CH_4 and (b) H_2 at *f*=40 kHz.

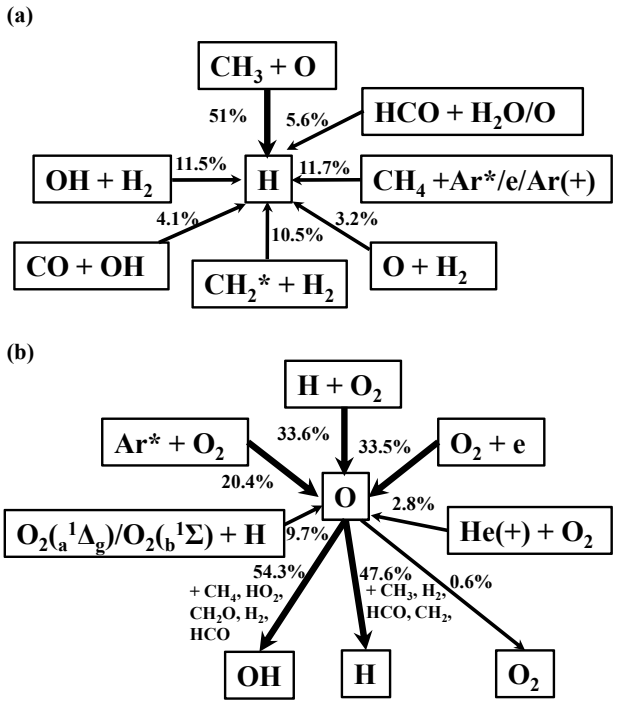

Figure 10. Reaction paths flux analysis for (a) H and (b) O at *f*=40 kHz.

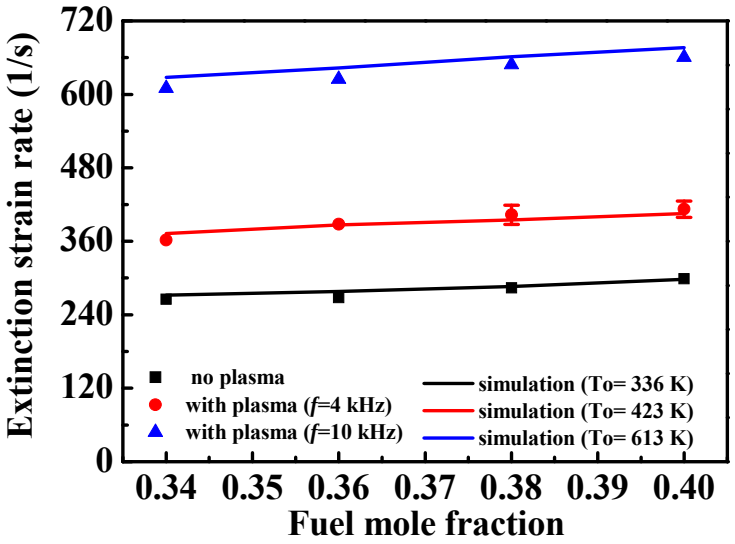

Figure 11. Relationship of extinction strain rate and fuel mole fraction under different experimental conditions.

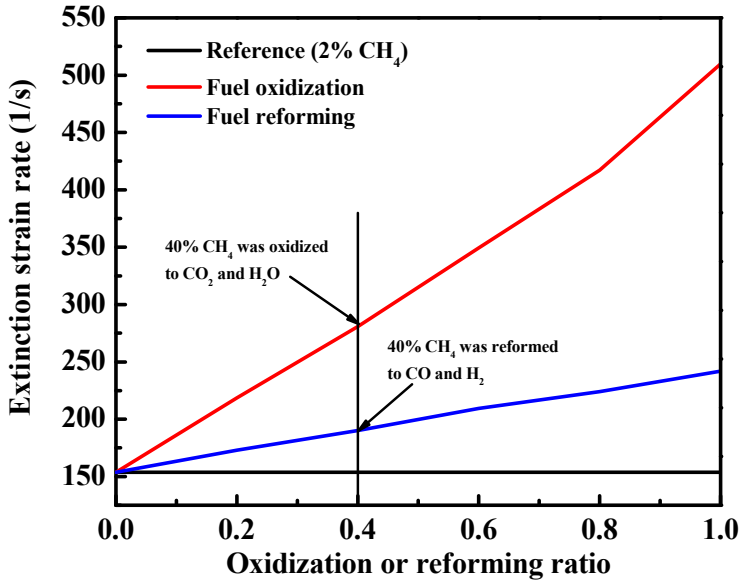

Figure 12. Comparison of extinction strain rates of fuel oxidization and fuel reforming effect at constant enthalpy condition for oxidizer stream Ar/He/O_2/CH_4 (0.32/0.4/0.26/0.02), *P*=60 Torr.

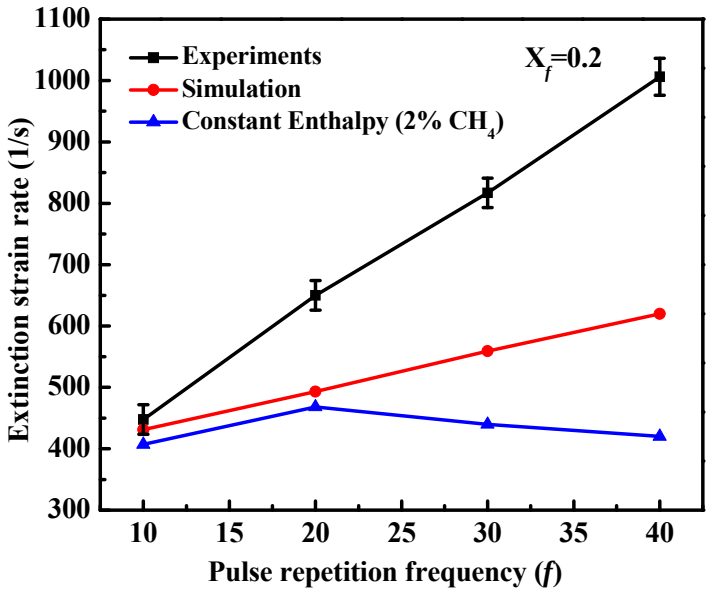

Figure 13. Relationship of extinction strain rate and pulse repetition frequency at X_f=0.2.

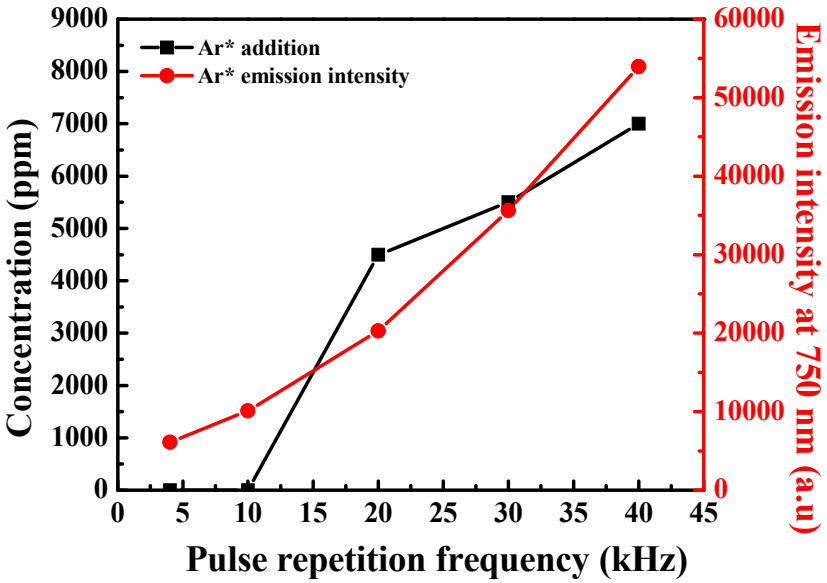

Figure 14. Relationship of required Ar* addition and emission intensity at 750 nm with pulse repetition frequency at X_f=0.2.